Available online at www.sciencedirect.com
SCIENCE DIRECT
Journal of Photochemistry and Photobiology A: Chemistry 180 (2006) 256–261
Journal of Photochemistry and Photobiology A:Chemistry
www.elsevier.com/locate/jphotochem

Optimal control methods applied on the ionization processes of alkali dimers

Albrecht Lindinger*, Stefan M. Weber, Andrea Merli, Franziska Sauer, Mateusz Plewicki, Ludger Wöste

Institut für Experimentalphysik, Freie Universität Berlin, Arnimallee 14, D-14195 Berlin, Germany

Available online 17 April 2006

Abstract

We present two novel optimization methods by employing shaped fs-laser pulses in a closed feedback loop. The first describes control pulse cleaning where extraneous features were removed by applying genetic pressure on certain pulse components. The second reports parametric optimization with intuitive parameters such as subpulse distances, chirps, phase differences, and spectral peak patterns. These methods were conducted on the ionization process of alkali dimers produced in a molecular beam and improved the performances of the optimized pulses compared with short pulses at the same pulse energy. Moreover, we attempt to analyze the obtained pulse shapes regarding the underlying optimized processes. Further investigations concerning isotope selective fragmentation and optimal control of excitation processes of ultracold rubidium dimers in a magneto-optical trap (MOT) are also shown.

PACS: 33.80.Rv; 28.60.+s; 82.53.−k

Keywords: Coherent control; Dimers; Parametrization

1. Introduction

Control of photo-induced molecular processes has attained considerable success in recent years. The development of pulse shapers, which allow to modulate laser pulses in the amplitude and phase domain, opened new perspectives for driving molecular reaction dynamics in real time. This topic became exciting when self-learning feedback loop algorithms with evolution strategies were employed [1]. In this way, tailored laser pulses can be generated which drive the photo-induced processes towards a maximum yield along desired paths via specific potential energy surfaces. A variety of optimization experiments were performed by several groups [2–11]. An important aspect remains the question concerning the information coded in the optimized laser pulse shape which could lead to a new approach regarding the investigation of molecular dynamics [10,12]. Employing evolutionary algorithms not only allows for an effective control of molecular dynamics by optimizing a problem of a high dimensionality but also supplies information about the involved molecular potential energy surfaces. Hence, it is important to study model systems where the molecular dynamics can be understood on the basis of theoretical evaluations. Larger systems with more degrees of freedom may then become experimentally controllable and understandable.

Alkali dimers are good model systems for optimal control studies because they have low ionization potentials with bound–bound electronic transitions utilized in resonant enhanced multiphoton ionization. Novel approaches to gain further information from the optimized laser field can favorably be implemented. One approach examines the implementation of genetic pressure within the algorithm for performing control pulse cleaning [13]. The aim is to remove extraneous pulse features in order to expose the most relevant structures and thus reveal mechanistic insights. The second method addresses parametric optimization [14] were the search space is narrowed down by introducing a few pulse parameter optimization. The suggested parameters in the time- and frequency-domain are time distances, intensities, zero order spectral phases, chirps of different subpulses, and spectral peak patterns. In this manner, the relevance of certain structural features of optimal pulses can be investigated.

This paper reviews the most recent investigations of these methods applied to cold alkali dimers, including the application

* Corresponding author.
E-mail address: lindin@physik.fu-berlin.de (A. Lindinger).

1010-6030/$ – see front matter © 2006 Elsevier B.V. All rights reserved.
doi:10.1016/j.jphotochem.2006.02.031

to ultracold atom ensembles, i.e. in a magneto-optical trap, in order to perform efficient control and to provide new insight. These latter studies can be seen as steps on a path to photoassociation of translationally cold atoms to molecules and vibrational cooling of the internal molecular degrees of freedom which would be promising issues regarding the production of quantum-degenerate molecular gases in particular vibrational states.

In the next section the experimental details of optimal control applied on a molecular beam are explained. Section 3 reports the results for the optimized ionization of NaK for free evolution, with the application of genetic pressure and for parametric optimization. The paper closes with expanded studies, a conclusion and an outlook.

2. Experimental

The NaK dimers are produced in an adiabatic co-expansion of the vapor from sodium/potassium alloy and argon carrier gas through a nozzle of 70 μm diameter into the vacuum [15]. The stagnation conditions of the molecular beam are chosen to produce NaK with no larger clusters present. Thereto, the oven temperature is set to about 600 °C and the argon pressure to 2.5 bars. After passing a skimmer, the molecular beam is directed between the electrical lenses of a quadrupole mass spectrometer (Balzers QMG 420), which are oriented perpendicular both to the propagation of the cluster beam and to the laser beam in order to extract the resulting photo-ions. A commercial femtosecond laser (Spectra Physics 3960 Tsunami), pumped by a Nd:YLF laser (Spectra Physics Millennia X), produces pulses of 120 fs duration, 6 nm spectral width, and 10 nJ energy per pulse at a central wavelength of 780 nm. Low pulse energies ensure that the laser-molecule interaction is well described in a perturbative picture and no high intensity effects have to be considered.

In the multi-photon optimization experiment, a laser beam passes through a pulse shaper setup, which allows for a simultaneous phase- and amplitude-modulation of the laser pulses by applying voltages to a liquid crystal spatial light modulator (SLM-256; CRI) consisting of 2 × 128 pixels. The shaper is placed in the center of a linear 4f arrangement. By computer control, pulses of arbitrary form can be generated. These modulated pulses are then focused on the molecular beam and the desired mass-selected product ion current is taken as a reference feedback signal. The optimization algorithm alters the pulse shaper settings iteratively in order to maximize the desired fitness. We apply an algorithm based on evolution strategies to find the pulse shape which yields the highest feedback signal. The optimization procedure continues until convergence is achieved. The generated optimized pulse form is measured by acquiring the pulse spectra, the cross-correlation, and the frequency resolved cross-correlation (XFROG).

3. Results and discussion

3.1. Phase-only optimization of the ionization of NaK

When maximizing the ionization of NaK we observed an almost monotonic rise of the ion yield during the optimization run.

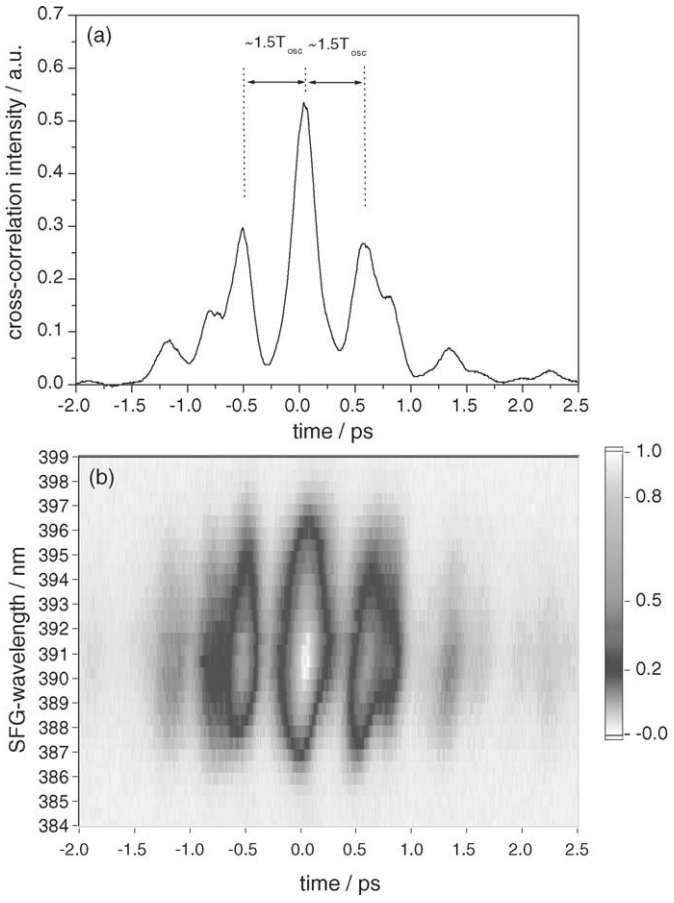

Fig. 1. Intensity cross-correlation (a) and XFROG trace (b) of the phase-only optimized pulse.

Convergence of the signal has been reached after approximately 120 iterations. In the presented free optimization only the phase was modified in order to keep the pulse energy constant.

The comparison of the ion yields between optimized and transform-limited pulses shows an improvement of the NaK^+ intensity by a factor of $I_{opt}/I_{tl} = 1.6$. An important feature of the molecular beam, visible in the recorded mass spectra, is the lack of any larger molecules which means that NaK ions originate only from NaK dimers and not from fragmented trimers, tetramers, or larger clusters. This result demonstrates the feasibility of optimizing the ionization process, however, we intended to move a step ahead and tried to learn from the optimized pulse shape about the underlying process. Therefore, we recorded the intensity cross-correlation and XFROG traces of the optimized pulse (Fig. 1). It contains three dominant and some smaller subpulses with time separations of almost 1.5 times the oscillation period of the first excited state ($T_{osc} = 440$ fs) [16]. The central pulse is thereby the most intense.

The relative intensities of the subpulses and their position in time suggest a simple scheme of ionization (see Fig. 2). The first peak transfers some population from the ground state to the first excited $A(2)^1\Sigma^+$ state. Due to the Franck–Condon principle and resonance conditions, the wavepacket is created at the inner turning point. After 1.5 oscillation periods in the $A(2)^1\Sigma^+$ state, it is located at the outer turning point where from it can be effectively

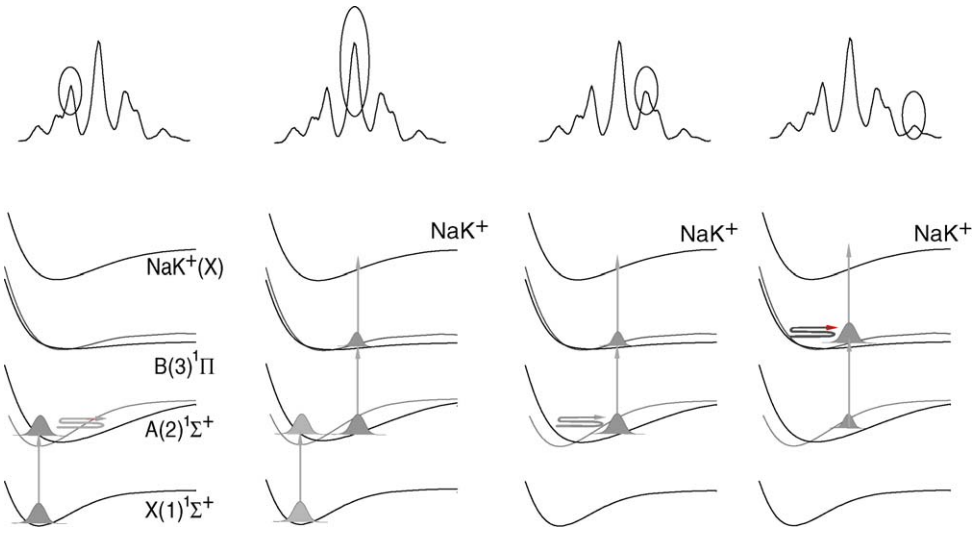

Fig. 2. Optimized photo-induced transition from the neutral ground state of NaK to the ionic ground state.

transferred to the ionic state. The second subpulse ionizes the molecule in a resonant two photon process and additionally generates a secondary wavepacket on the first excited state. Again, after the second wavepacket is located at the outer turning point, it is being transferred to the ionic state by the third subpulse. The second excited state $B(3)^1\Pi$ state will also be populated by the second and third subpulse. A fourth weak subpulse may transfer the residual population from the first and second excited state to the ionic state. Also the propagation in the $B(3)^1\Pi$ state with an oscillation period of about 700 fs is included in the ionization process. This explanation is supported by full quantum-mechanical calculations of the optimization process undertaken in the group of Prof. Bonačić-Koutecký for the slightly different center wavelength of 770 nm. They solved the optimization functional by iteration until self-consistency was achieved and we observed a qualitative agreement between the theoretically and experimentally acquired optimized pulses [17]. Snapshots of the wavepacket propagations revealed the explained mechanism and showed that the wavepacket oscillation in the $B(3)^1\Pi$ state occurs as well within the ionization process. Moreover, it was found that later smaller subpulses contribute much to the overall ion yield since they are responsible for the last excitation step to the ionic state. In our experiment we expect a similar behavior for the only slightly shifted center wavelength. Constructive interferences of the molecular wavepackets in the excited states as mentioned in Ref. [17] are presumably also utilized in the optimized ionization path for 780 nm center wavelength. Thus, it is found that basically a stepwise excitation takes place in the optimized ionization process.

3.2. Control pulse cleaning

A novel method in coherent control named control pulse cleaning describes the process of removing extraneous control field features in a closed-loop quantum dynamics optimization experiment. This is accomplished by applying genetic pressure during the optimization run in order to simplify the optimized pulses and to reveal the most relevant features. Thereto, a new fitness function has to be formed where the target goal f is optimized and simultaneously genetic pressure is implemented on certain pulse components. We solved this for the NaK model system by introducing the fitness function $F = f/((1/N)\sum_{l=0}^{N} T_l)^{\gamma}$ with the transmissions T_l with $l = 1, 2, \ldots, N$ for all $N = 128$ pixels. The weighting exponent γ can be freely chosen to set the desired degree of genetic pressure. The phase values were thereby allowed to be modulated freely without genetic pressure.

The inset of Fig. 3 shows the spectrum (solid line) and the pixel transmissions (grey bars) of the optimized pulse with $\gamma = 1.5$ for the slightly different center wavelength of 770 nm. It exposes otherwise not visible vibronic transitions to the first and

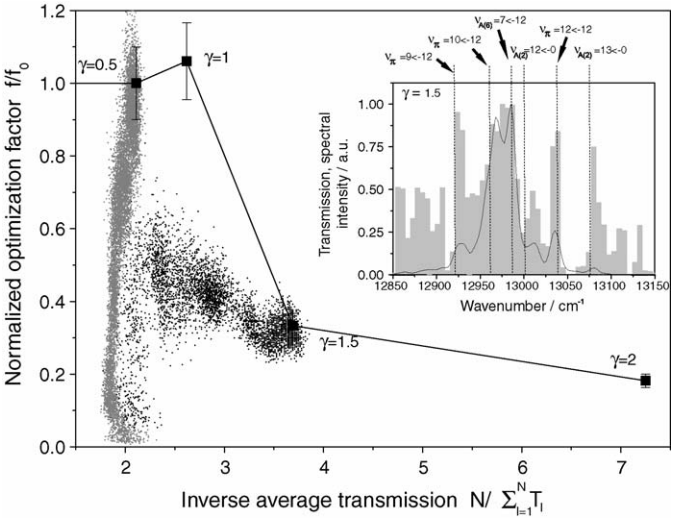

Fig. 3. Correlation plot of the normalized optimization factor f/f_0 vs. the inverse average transmission. The solid line depicts the estimated Pareto-optimal front drawn through the optimal solutions for different γ. The optimization courses for $\gamma = 0.5$ (grey points) and $\gamma = 1.5$ (black points) are shown by plotting the values of every individual. The inset shows the spectrum (solid line), and the pixel transmissions (grey bars) of the optimized pulse for $\gamma = 1.5$. Vibronic transitions to the first and second excited states are denoted.

second excited states. This demonstrates the feasibility of control pulse cleaning and shows that otherwise hidden information can be unraveled.

Fig. 3 depicts a correlation plot of the normalized optimization factor f/f_0 and the inverse average transmission. Plotted is the so called Pareto-optimal front (solid line) drawn through the optimal solutions for different γ. As examples, the optimization courses for $\gamma = 0.5$ (grey points) and $\gamma = 1.5$ (black points) are shown by plotting the values of every individual. Both optimizations evolve from the lower left to the upper right. While the ion yield increases at almost constant transmission for the optimization with $\gamma = 0.5$, the optimization for $\gamma = 1.5$ first tends to increase f/f_0 and then decreases by proceeding to lower average transition which indicates the enhanced efficiency of cleaning at the end of the optimization. This concept may be generalized to multi-criterion optimizations with several physical relevant objectives and new algorithms could be utilized where one receives the entire Pareto-optimal front within one run.

In the following, a different approach to receive further information will be applied by performing a few parameter optimization, where the search space is reduced to permit only simple pulse trains or spectral patterns. In this manner the relevance of certain structural features of the optimized pulses can be investigated.

3.3. Parametric optimization of NaK ionization in the time domain

A further advantage of parametric optimization, besides search space reduction and application of physically relevant and intuitive parameters, is the possibility to define the framework of an experiment. One can for example choose a parameter set for an intended purpose and will receive the optimized result within this parameter set. Here, we asked the question what will be the result if we allow different numbers of subpulses, which will tell us the relevance of the additional subpulses. Thereto, we constructed the complex electrical field of a pulse train after passing the shaper by

$$\tilde{E}_{\text{out}}(t) = \mathrm{e}^{i\omega_0 t} \sum_n \varepsilon_n(t - t_n)\, \mathrm{e}^{i\varphi_0 t} = \mathrm{e}^{i\omega_0 t} \sum_n \tilde{\varepsilon}_n(t - t_n) \qquad (1)$$

with ε and $\tilde{\varepsilon}$ being the field envelope and complex field envelope of the subpulses, respectively, and t_n being the time distances between the subpulses. The resulting temporal field is then Fourier-transformed to receive an electrical field in the frequency description. The desired output for the electrical field is hence produced from the modulator by writing the filter function $\tilde{H}(\omega) = \tilde{E}_{\text{out}}(\omega)/\tilde{E}_{\text{in}}(\omega)$. The experiments were performed by pure phase modulation in order to keep the total pulse energy constant. We reduced the full search space to an 11 or 23 parameter space for three or six subpulses, respectively, where the subpulse distances, intensities, constant phase differences, and linear chirps between were subject to optimization. Fig. 4 shows the SFG cross-correlation results for optimizing three (a) or six (b) subpulses. The acquired pulseforms of three different runs are presented in (a) in order to test the robustness of the optimized pulse shape. Particular subpulse distances corresponding to $1.5T_{\text{osc}}$ can be observed for all runs. However, the optimization factor increased from approximately 1.2 for three subpulses to about 1.5 for six subpulses, which comes closer to the value of 1.6 for free optimization. This indicates that apparently more than three subpulses are required for an efficient transfer to the ionic state, which is in concordance to the model explanation given above. We allowed linear chirps of the subpulses between -20000 and 20000 fs^2 which may further enhance the ion yields. Due to inherent uncertainties of the chips we abstained from interpreting them in detail and explained only the clear hints regarding the number and spacings of the subpulses. The unre-

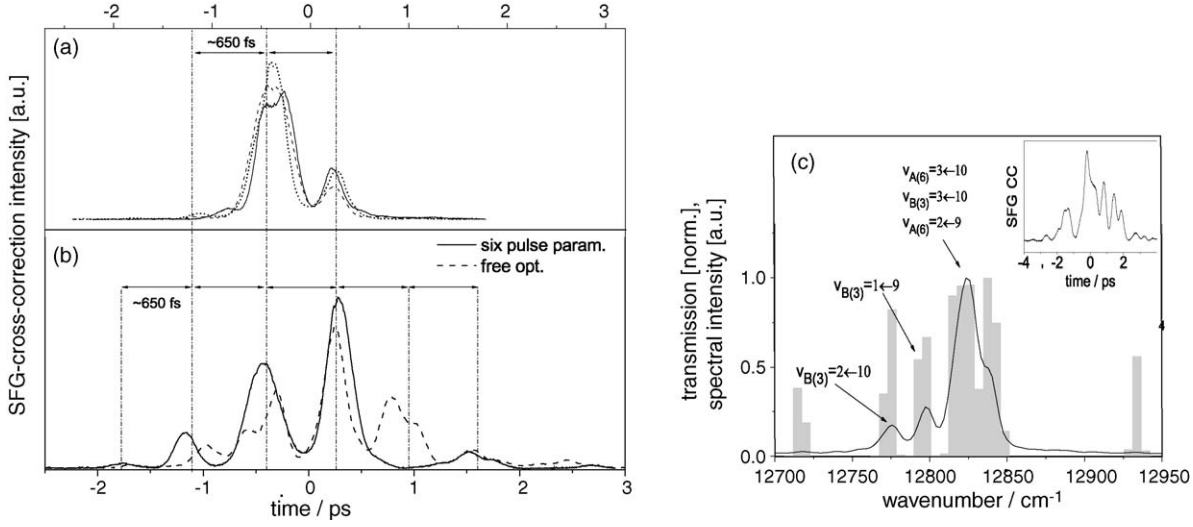

Fig. 4. The SFG cross-correlation results are shown for optimizing three (a) or six (b) subpulses (solid line). The results of three different runs are shown in (a). Subpulse distances of 650 fs corresponding to $1.5T_{\text{osc}}$ are visible in all cases. The optimized pulse for free optimization is shown in (b) as a dashed line. The spectrum of the optimized pulse for parametrization in the frequency domain employing 11 narrow Gaussian distributions is shown in (c) (the inset depicts the cross-correlation trace). The spectral peaks are assigned to vibronic transitions.

stricted optimization produced a comparable waveform except for one more subpulse at around 0.8 ps. The remaining difference between the parametric and the free optimization may further originate from the search space restriction since some pulse components were still not modulated in the parametric case. Yet, this example shows the potential of the introduced method to gradually gain knowledge about the molecular system.

Another possibility is to perform spectral parametrization, where narrow Gaussian amplitude distributions are subject to modulation in order to find certain vibronic transitions. Parameters are the distances and intensities of these distributions. The phase can thereby be modulated freely to allow unrestricted temporal pulse modulation, as realized here. For the NaK model system we were able to find some involved transitions to the first and second excited state (see Fig. 4(c)). This so called transition finder can generally be applied to search for those transitions in molecular systems which are utilized by the optimized path.

3.4. Further investigations

As an example of multi-objective optimizations with physically relevant parameters we performed isotope selective optimization on the K_2 model system. When we only optimized the $^{39}K/^{41}K$ atom ion ratio by free phase and amplitude modulation for different center wavelengths in a first experiment, we astonishingly exposed molecular fingerprints in the optimized pulse forms which could be assigned to vibronic transitions within the dimer [18]. One does not expect to influence the two atomic potassium isotopes differently with pulse structures no shorter than 120 fs, since only the much faster electron dynamics may exhibit minor differences. Thus, only the molecular features can be related to the distinct pulse structures.

In order to perform two criteria optimizations we maximized the fragment versus the dimer ion isotope ratio with selected weighting factors. The new fitness function, chosen as the weighted sum of the ratios, is expressed as

$$F = (1-\beta)\left[\frac{I(^{39,39}K_2^+)}{I(^{39,41}K_2^+)}\right] + \beta\left[\frac{I(^{39}K^+)}{I(^{41}K^+)}\right] \quad (2)$$

with the weighting factor β. The fitness function is chosen in such a way that three regimes are achieved by modifying only one weighting parameter. For $\beta < 0$ the isotopomer ion ratio is optimized at the cost of the fragmentation ion ratio, for $0 < \beta < 1$ both goals are optimized simultaneously, and for $\beta > 1$ the fragmentation is favored at the cost of the dimer isotopomer ionization. Hence, this choice allows a gradual increase of the fragmentation/ionization character by modifying β. Genetic pressure can therefore be applied in both directions, fragmentation and dimer ionization.

Several maximizations were conducted for different values of β at 810 nm center wavelength (chosen because of its highest fragmentation factor). Fig. 5(a) shows the ratio between $I(^{39}K^+)/I(^{41}K^+)$ and $I(^{39,39}K_2^+)/I(^{39,41}K_2^+)$ as a function of the weighting factor β. An increase of this ratio with rising β is visible. This shows that the processes are influenced as intended by the choice of β and that the two goals are apparently not strongly conflicting. As we observed for large β (i.e. enforced fragmentation) indications of vibronic transitions to the two involved molecular excited states we conclude that the fragmentation takes place in the ionic dimer state. Apparently, the repulsive state $K_2{}^+\,{}^2\Sigma_u^+$ (shown in Fig. 5(b)) is reached in the optimized process leading to enhanced fragmentation.

Another prospective application of optimal control is the interaction of shaped laser pulses with ultracold atoms and molecules in a magneto-optical trap (MOT) in order to do photoassociation of atoms to molecules or vibrational cooling of the present molecules. We performed first steps on this way by controlling the excitation processes of ultracold rubidium dimmers

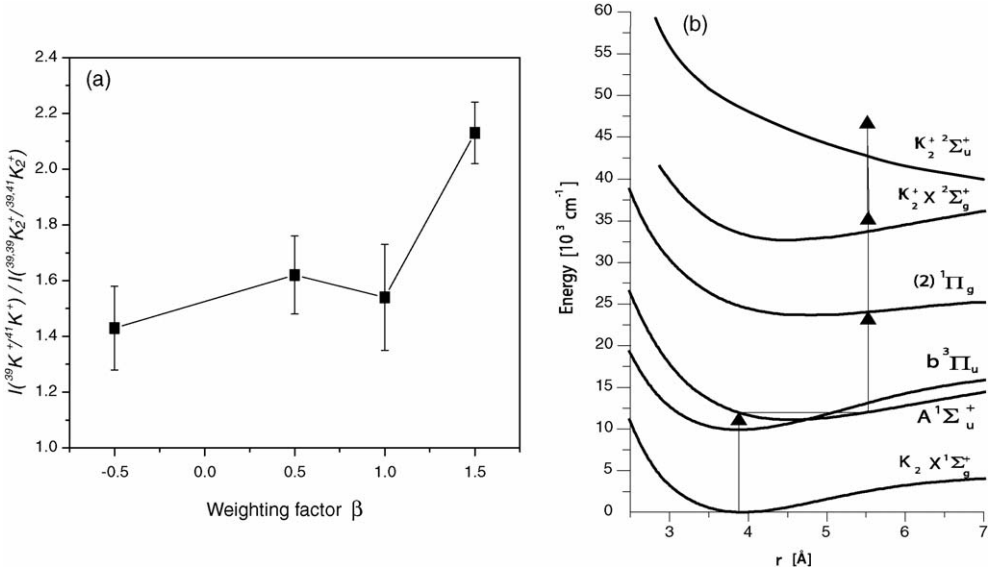

Fig. 5. (a) Optimization results for the ratio between $I(^{39}K^+)/I(^{41}K^+)$ and $I(^{39,39}K_2^+)/I(^{39,41}K_2^+)$ vs. the weighting factor β by employing the fitness function $F = (1-\beta)[I(^{39,39}K_2^+)/I(^{39,41}K_2^+)] + \beta[I(^{39}K^+)/I(^{41}K^+)]$. (b) Potential energy diagram for K_2 and presumed optimized path.

in a ^{85}Rb MOT (see Ref. [19] for details). By closing the loop we were able to deplete the existing molecules more efficiently than by using a short pulse of the same pulse energy. For this optimization we used a parametrization in the frequency domain where the parameters of several narrow Gaussian peaks were optimized. In order to allow shaping in the temporal domain the phase values were subject to free optimization. Unfortunately, the stability and the signal-to-noise ratio allowed only partial optimizations, yet the most relevant information could be extracted from several runs. The spectra of the optimized pulse shapes of different runs showed distinct peaks at almost the same positions. This may be explained by vibronic transitions to the first excited triplet state but the measured frequency spacing is larger than the difference between adjacent vibrational levels in the excited state. Apparently, Franck–Condon factors may also play a role since their value oscillates with about the same frequency spacing as in the obtained spectra. Since the frequency parametrization is essential for the observation, this application demonstrates the potential of parametric optimizations.

4. Conclusion and outlook

We reported two optimization methods on alkali dimer model systems by using shaped fs-laser pulses in a feedback loop. One approach presented control pulse cleaning where extraneous pulse features were removed by applying genetic pressure during the optimization. Involved vibronic transitions to the first and second excited states were exposed and the general concept of Pareto-optimal solutions was introduced. This demonstrates the feasibility of control pulse cleaning and shows that otherwise hidden information can be unraveled. The second method utilizes parametric optimization with intuitive parameters such as subpulse distances, chirps, phase differences, and spectral peak patterns. The results revealed, e.g. the dependence of the ionization yield on the number of subpulses or exposed the involved vibronic transitions.

Further investigations were presented concerning the multicriterion optimization of ionization versus fragmentation and optimal control of excitation processes of ultracold rubidium dimers in a magneto-optical trap (MOT). Yet, several questions remained open for the latter example and are planned to be investigated in an improved design with a considerably larger production rate of ultracold molecules and a higher detection rate. A close cooperation with theory will help to find particular pulse shapes for these processes [20]. It is also envisioned to try to cool the molecules to their vibrational ground states by pump-dump like processes via an intermediate excited state. Moreover, the use of longer shaped pulses may be employed to perform photoassociation and cooling simultaneously. The application of a higher resolving pulse modulator is already in preparation which allows an improved frequency resolution and a more complex temporal pulse modulation for precisely addressing the vibrational energy levels. The application of coherent control for steering fundamental processes in ultracold ensembles like photoassociation and vibrational cooling is prospective, since it can be regarded as an essential step on the path to an internally cold molecular Bose–Einstein condensate.

Acknowledgments

The authors thank B. Schäfer-Bung, V. Bonačić-Koutecký, H. Rabitz, W. Salzmann, R. Wester, and M. Weidemüller for stimulating ideas and discussions. F. Sauer acknowledges the Studienstiftung des deutschen Volkes. A. Merli thanks the Cusanuswerk. The DFG supported this work in the frame of the SFB 450.

References

[1] R.S. Judson, H. Rabitz, Phys. Rev. Lett. 68 (1992) 1500.
[2] C.J. Bardeen, et al., Chem. Phys. Lett. 280 (1997) 151.
[3] A. Assion, et al., Science 282 (1998) 919.
[4] D. Dantus, V.V. Lozovoy, Chem. Rev. 104 (2004) 1813.
[5] T. Hornung, R. Meier, M. Motzkus, Chem. Phys. Lett. 326 (2000) 445.
[6] S.A. Rice, Science 258 (1992) 412.
[7] R.J. Levis, G.M. Menkir, H. Rabitz, Science 292 (2001) 709.
[8] A. Lindinger, C. Lupulescu, M. Plewicki, F. Vetter, A. Merli, S.M. Weber, L. Wöste, Phys. Rev. Lett. 93 (2004) 033001.
[9] H. Rabitz, R. de Vivie-Riedle, M. Motzkus, K. Kompa, Science 288 (2000) 824.
[10] Š. Vajda, et al., Chem. Phys. 267 (2001) 231.
[11] R. Bartels, et al., Nature 406 (2000) 164.
[12] A. Bartelt, A. Lindinger, Š. Vajda, C. Lupulescu, L. Wöste, Phys. Chem. Chem. Phys. 6 (2004) 1679.
[13] J.M. Geremia, W. Zhu, H. Rabitz, J. Chem. Phys. 113 (2000) 10841.
[14] S.M. Weber, A. Lindinger, F. Vetter, M. Plewicki, A. Merli, L. Wöste, Eur. Phys. J. D 33 (2005) 39.
[15] A. Bartelt, S. Minemoto, C. Lupulescu, Š. Vajda, L. Wöste, Eur. Phys. J. D 16 (2001) 127.
[16] L.-E. Berg, M. Beutter, T. Hansson, Chem. Phys. Lett. 253 (1996) 327.
[17] B. Schäfer-Bung, R. Mitric, V. Bonačić-Koutecký, A. Bartelt, C. Lupulescu, A. Lindinger, Š. Vajda, S.M. Weber, L. Wöste, J. Phys. Chem. A 108 (2004) 4175.
[18] A. Lindinger, A. Merli, M. Plewicki, F. Vetter, S.M. Weber, L. Wöste, Chem. Phys. Lett. 413 (2005) 315.
[19] W. Salzmann, U. Poschinger, R. Wester, M. Weidemüller, A. Merli, S.M. Weber, F. Sauer, M. Plewicki, F. Weise, A. Mirabal Esparza, L. Wöste, A. Lindinger, Phys. Rev. A 73 (2006) 023414.
[20] C. Koch, R. Kosloff, F. Masnou-Seeuws, online available at: arXiv:physics/0511235v1.